Rheology of Marine Sponges Reveals Anisotropic Mechanics and Tuned Dynamics

Emile A. Kraus,[1] Lauren E. Mellenthin,[2] Sara A. Siwiecki,[3] Dawei Song,[4,5] Jing Yan,[6,7] Paul A. Janmey,[1,4,5] and Alison M. Sweeney[2,7,8]

[1)] *Department of Physics & Astronomy, University of Pennsylvania*

[2)] *Department of Ecology & Evolutionary Biology, Yale University*

[3)] *Department of Mol. Biophysics & Biochemistry, Yale University*

[4)] *Institute for Medicine & Engineering, University of Pennsylvania*

[5)] *Department of Physiology, University of Pennsylvania*

[6)] *Department of Mol., Cell., & Dev. Biology, Yale University*

[7)] *Quantitative Biology Institute, Yale University*

[8)] *Department of Physics, Yale University*

Sponges are animals that inhabit many aquatic environments while filtering small particles and ejecting metabolic wastes. They are composed of cells in a bulk extracellular matrix, often with an embedded scaffolding of stiff, siliceous spicules. We hypothesize that the mechanical response of this heterogeneous tissue to hydrodynamic flow influences cell proliferation in a manner that generates the body of a sponge. Toward a more complete picture of the emergence of sponge morphology, we dissected a set of species and subjected disks of living tissue to physiological shear and uniaxial deformations on a rheometer. Various species exhibited rheological properties such as anisotropic elasticity, shear softening and compression stiffening, negative normal stress, and non-monotonic dissipation as a function of both shear strain and frequency. Erect sponges possessed aligned, spicule-reinforced fibers which endowed three times greater stiffness axially compared with orthogonally. By contrast, tissue taken from shorter sponges was more isotropic but time-dependent, suggesting higher flow sensitivity in these compared with erect forms. We explore ecological and physiological implications of our results and speculate about flow-induced mechanical signaling in sponge cells.

Keywords: rheology, marine sponges, tissue mechanics, anisotropic elasticity, auxeticity, nonlinear viscoelasticity

I. INTRODUCTION

Sponges, animals that branched near the root of the metazoan tree [1, 2], are a successful and unique phylum despite perceived simplicity since they have no muscles nor nerves [3, 4]. The extracellular part of their bodies is a highly efficient fluid transport system made of diverse collagen-like proteins (spongins) and stiff organomineral inclusions called spicules [5]. Inner chambers of sponge tissue are lined with flagellated collar cells whose waving flagella draw ambient water in through small surface pores (ostia) on the sponge body. The water travels through narrowing canals, is filtered of dissolved nutrients, and then leaves through widening canals until exiting from larger, apical holes (oscula). Famously, sponges vary vastly in size and shape, appearing in almost all aquatic niches and flow regimes as globs, cups, vases, carpets, fans, barrels, spheres, fingers, and tall trees. How they grow and sustain bodies presumably optimized for transport of matter in these various niches is not fully understood, thus physical characterization of their tissue is necessary.

Like snowflakes, no two sponges are exactly alike, and this dizzying diversity likely arises from interactions among an individual's tissue mechanical properties, the hydrodynamics of its environment, and mechanical signaling of its cells. Early spongiologists knew that sponges of smaller diameter piping generate larger pump pressures which send filtered water further [6]. This lowers the probability of water recirculation but increases the frictional cost of transport through the sponge [7]. G.P. Bidder in particular, documented that thin-tissued, deep-sea glass varieties of sponge ~~would~~ have lower internal pressure than their denser, shallow-water cousins [6, 7]. The tissue elasticity of these dense sponges counteracts ambient pressure and flow-induced stresses in mechanical equilibrium. However, no explicit measure of these elastic properties across sponge groups has yet been made.

An ecological study of the encrusting sponge *H. panicea*, placed its tissue stiffness (elasticity) between 200 and 600 kPa, and proportional to wave-induced stresses up to 10 kPa [8]. Steady, flow-induced forces like drag and lift, impart highly morphology-dependent stresses on the bodies of sessile aquatic animals. However, sponges of different body forms are often found next to each other (Fig. S3), such that there isn't a simple form vs. ambient flow relationship in these animals. Tissue mechanical properties then, must also be tuned by evolution and development in specific sponges. Other invertebrates with fixed body forms and static mechanical properties such as mussels, urchins, and limpets, have a strict upper

limit on their size in fast and accelerating (i.e. time-dependent) flows [9]. It is less clear what mechanical constraints apply to sponges, given their asymmetrical body plan and lack of internal organs, or whether there are aspects of sponge tissue that enable mechanical responsiveness to environmental flow.

Monactine sponge spicules are known to have extreme resistance to buckling failure under compression [10], but it is not understood how their arrangement within a cellular and fibrous protein network contributes to the mechanical whole of sponge tissue. Gelatin hydrogels embedded with spicules have stiffnesses proportional to the volume fraction of these stiff inclusions, as well as strain-softening dynamics [11], but did not contain sponge cells capable of creating internal strain or otherwise affecting tissue rheology.

We thus take a holistic approach by performing rheology on living tissue from several common sponge species. We applied small to moderate strains over a frequency range salient to the properties of environmental flows and stresses. The mechanical and dynamical (i.e. time-dependent) properties of sponge tissue measured in this way correlate to their growth morphologies and skeletal structures. We speculate that the stiff skeleton and its coupling to living sponge cells, generates mechanical cues that in turn influence cell proliferation, just as extracellular matrix mechanics modulate many cell physiological processes in mammalian tissues [12, 13]. The sponge rheologies presented showcase tissue mechanical diversity, and in some species, rich nonlinear viscoelasticity at relatively small strains compared with *in vitro* and mammalian systems.

II. MATERIALS & METHODS

A. Animal Care & Sample Preparation

Sponges were procured from Gulf Specimen Marine Laboratories (Panacea, FL) and acclimated slowly by drip to a large, 1-m depth (ESM 4) laboratory saltwater aquarium (T = 20 degrees C, salinity 36 g/kg). We chose individuals with open oscula and bright tissue for preparing samples, as these characteristics indicate good health. All sponges were used within a span of several weeks and any exposure to air was minimized. We used a kitchen sponge (Medium Duty, Scotch-Brite) to determine whether living sponge rheology was distinct from that of a synthetic porous material. For branching and erect species of

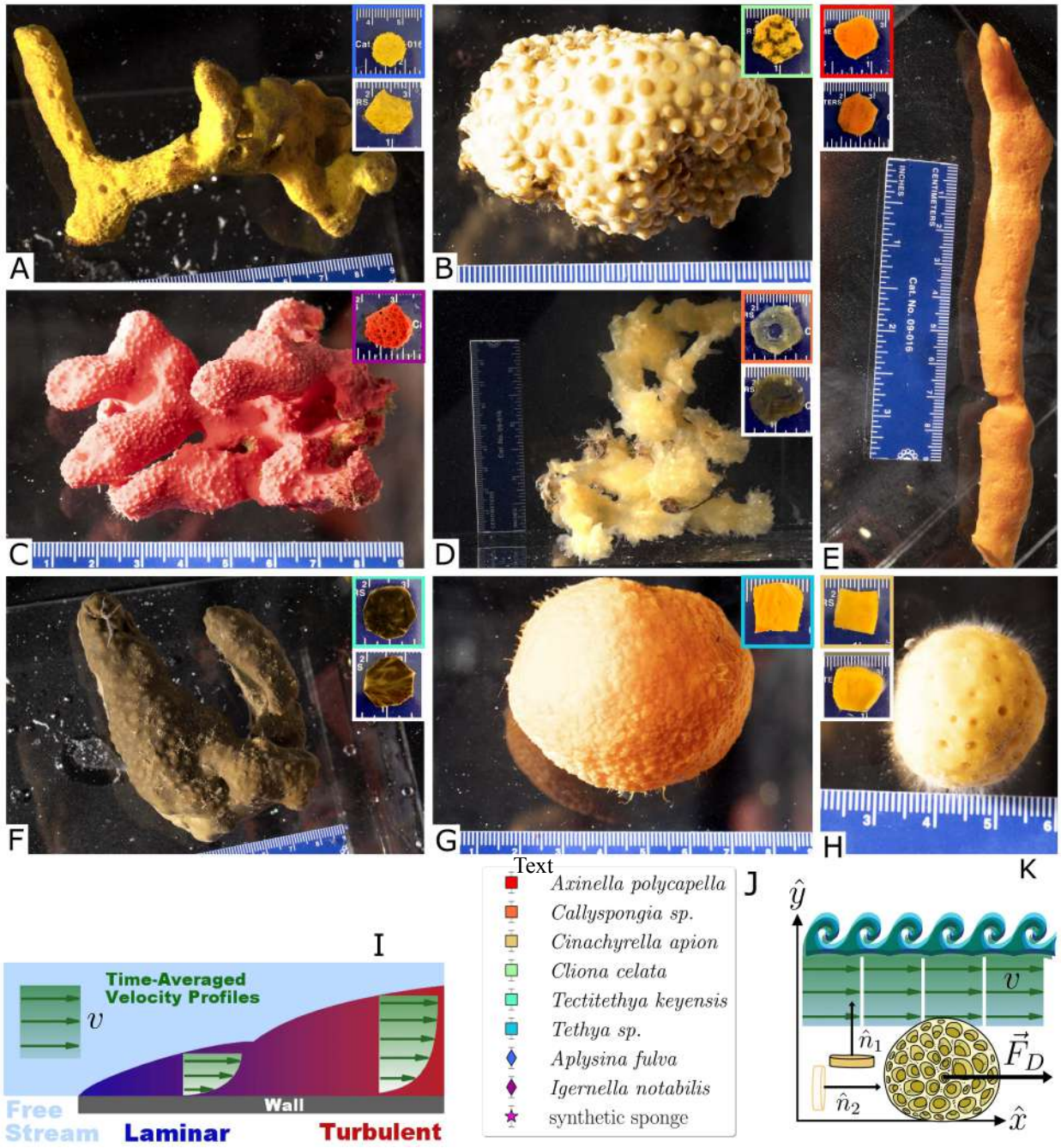

FIG. 1. Sponges studied. A) *A. fulva* B) *C. celata* (gamma growth form [14]) C) *I. notabilis* D) *Callyspongia sp.* E) *A. polycapella* F) *T. keyensis* G) *Tethya sp.* H) *C. apion.* Images of representative sample disks for rheology are inset. I) Diagram (courtesy of Symscape) of ambient flows: steady flow v (left) and boundary layer flow (right). J) Key of sponges: squares have spicules, diamonds do not. K) Schematic of sampling geometry in relation to v and subsequent drag $\vec{F}_D$ on an example sponge. $\hat{z}$ points into the page.

Usually you can't put citations in figure legends. It is also not clear what "courtesy of Symscape" means. Can you just redraw a simpler version of this in Illustrator to avoid the slight cheesiness of re-using a random internet gif? Also, the stuff in the caption for panel I doesn't really match what's in the image.

sponge, tissue cuts parallel to their substrate attachment area were made with a razor blade, resulting in disks of thickness 2–4 mm with axial vectors $\hat{n}_1$ parallel to $\hat{y}$ and perpendicular to ambient flow v as depicted in Fig. 1K. We also made cuts perpendicular to the substrate, so that these disks' axial vectors $\hat{n}_2$, were oriented along $\hat{x}$. In species where consistent samples could not be obtained in the above fashion due to tissue being too heterogeneous (*C. celata*), compressible (*I. notabilis*), or brittle (pith of *Tethya sp.*), a biopsy device was used to punch 12–14 mm diameter cylindrical cores which were then sliced into disks of thickness 2–4 mm. Disks from different cores were thus distinctly oriented at random with respect to ambient flow v, so we denote their axial vectors $\hat{n}_{\blacksquare}$, $\hat{n}_{\blacksquare}$, and $\hat{n}_{\blacksquare}$.

Sponges can be difficult to identify to species, and our experimental animals were obtained from a commercial supply source. All species sampled here were demosponges, and species identifications are provided to the best of our ability in working with this supply resource. In this instance, photographs of the individuals used and their spicules are included, and are the best information we have about exact species identity. Ultimately, the magnitude and quality of the differences between individuals and species are the most salient part of the present work.

B. Rheology

We mounted disks of live sponge tissue between parallel plates (12 mm diameter) on a rheometer (MCR 502 WESP, Anton Paar GmbH). A small amount of cyanoacrylate adhesive (Gorilla Super Glue Gel 7700104) was applied to both sides of the sample to maintain contact between it and the rheometer plates during deformation. We initialized contact with the plates by exerting a uniaxial stress $\sigma_N \sim 10$ kPa, and the sample was then immediately rewetted with 1 mL of artificial seawater (Fig. 2A). We did not observe the living tissue react or degrade with the glue application, and the resulting film formed could be peeled off intact after the experiments. Therefore, the use of this adhesive does not seem to have altered any internal properties of the sponge tissue.

After relaxation of the loading stress, we applied sinusoidal shear strain

$$\gamma(t) = \gamma_0 \sin(\omega t) \tag{1}$$

where γ_0 is the strain amplitude and ω is the angular frequency (speed) of oscillation (Fig. 2B). For small γ_0, such that stress outputs are proportional to strain inputs, the shear

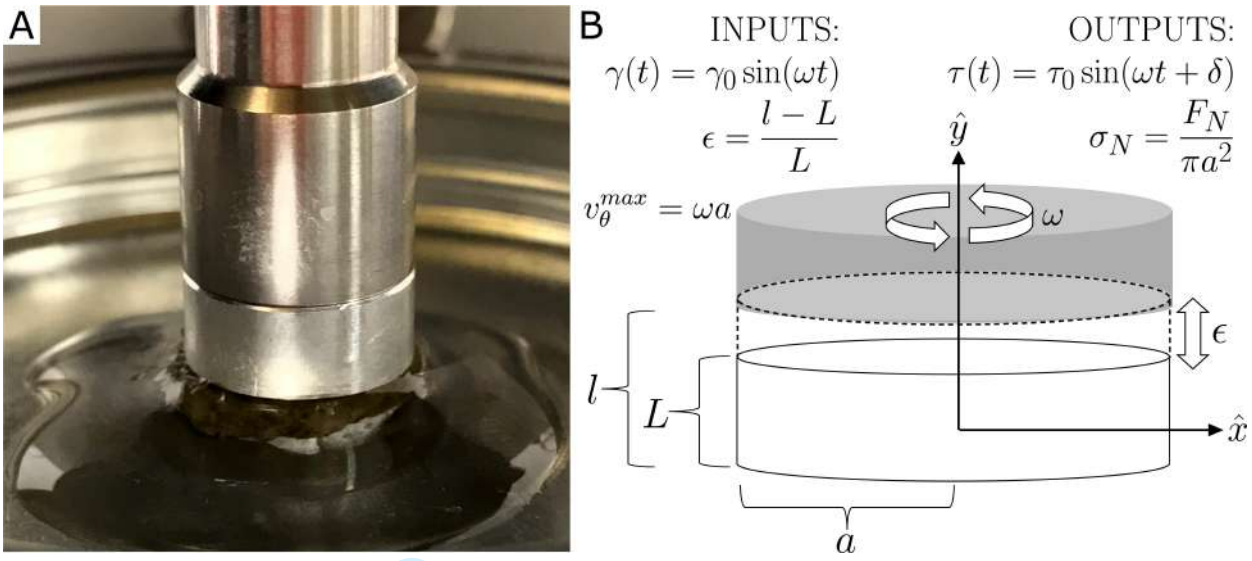

FIG. 2. Rheometry schematic. A) sample in the rheometer. B) parallel-plate geometry (radius $a = 0.6$ cm), used to impose oscillatory shear $\gamma(t)$ and uniaxial strain ϵ.

stress in the sample $\tau(t)$ is a single sinusoid shifted by an amount δ

$$\tau(t) = \tau_0 \sin(\omega t + \delta) \tag{2}$$

where τ_0 is the shear stress amplitude. The dynamic storage and loss moduli, $G'(\omega)$ and $G''(\omega)$, quantify elastically stored and viscously dissipated energy due to oscillatory shear and describe a sample's viscoelastic response in the linear regime. We measured $G'(\omega)$, $G''(\omega)$, and their ratio $\tan\delta = G''/G'$ at twelve logarithmically spaced frequencies between 0.1π and 10π s^{-1} at $\gamma_0 = 0.05\%$. Ambient, free-stream flow v (Fig. 1I) in marine intertidal and subtidal environments where sponges are common typically ranges from 0.1 to 100 cm s^{-1} [8, 9]. Since the maximum speed v_θ of a disk-shaped sample subject to torsion is $v_\theta^{max} = \omega a$ [15] where a is the disk radius, we chose these frequencies ω as they correspond to environmentally-relevant flow speeds between 0.2 and 20 cm s^{-1}.

We interpreted the linear viscoelasticity of sponge tissue, as characterized by our frequency sweep data, using rheological circuit models. We considered the classical Maxwell, Kelvin-Voigt, and Zener models, as well as a model with a fractional-order derivative element known as a spring-pot [16]. This fractional calculus-based model was formulated to capture precisely, and without overfitting, the power-law viscoelasticity commonly seen in biological materials [16]. Fits were performed with the Julia (v1.5.3) package RHEOS, developed for robust optimization of linear viscoelastic data [17].

After a frequency sweep, we subjected samples to steady uniaxial strain or large-amplitude oscillatory shear (LAOS). We conducted LAOS on a subset of species by increasing shear strain, γ_0, in twelve logarithmic increments from 0.1 to 10% at $\omega = 4\pi$ s^{-1}. To check for any pre-conditioning effects, we repeated this LAOS protocol after ten minutes of rest. We were unable to probe above $\gamma_0 = 10\%$ in *A. polycapella* and *C. celata* and $\gamma_0 = 20\%$ in *Callyspongia sp.*, since the glue typically separated from the rheometer plates prior to any visible sample failure. Sponges in nature are not regularly observed to deform in ambient flow, so we considered $\gamma_0 = 20\%$ a reasonable value to qualitatively capture strains that are not readily perceptible, and above which, strains are unlikely to be physiological.

Within the nonlinear viscoelastic regime probed by LAOS experiments, higher harmonics of the driving (fundamental) frequency are excited in a material's mechanical response. In other words, the stress output in the sample $\tau(t)$ is no longer a single sinusoid shifted in time from the input strain $\gamma(t)$ but can be represented as a Fourier series taken over odd-integer harmonics n due to the odd symmetry of shearing.

$$\tau(t) = \gamma_0 \sum_{n:odd} \left(G'_n(\omega, \gamma_0) \sin n\omega t + G''_n(\omega, \gamma_0) \cos n\omega t \right) \quad (3)$$

Here, ~~where~~ $G'_n(\omega, \gamma_0)$ and $G''_n(\omega, \gamma_0)$ ~~are now~~ become a set of trigonometric Fourier coefficients. Material measures may also be extracted from parametric plots of $\tau(t)$ vs. $\gamma(t)$, or elastic Lissajous-Bowditch (L-B) curves [18]. For amplitudes γ_0 within the linear regime, L-B curves are ellipses and $G'(\omega)$ and $G''(\omega)$ are proportional to the semi-major and semi-minor axes [19]. In the nonlinear regime, L-B curves become bent shapes whose axes are no longer constant with respect to $\gamma(t)$. This distortion of L-B curves is a geometrical signal that the linear moduli $G'(\omega)$ and $G''(\omega)$ are insufficient to describe a sample's viscoelastic nonlinearities [18].

Here, we analyze the nonlinear $\tau(t)$ signal in sponges with the minimum strain $G'_M(\gamma_0)$ and maximum strain $G'_L(\gamma_0)$ elastic moduli because together they describe an L-B curve's overall concavity and moreover, are analytically related to $G'_n(\omega, \gamma_0)$ (Eqn. S5) [18, 19, 20]. We compare $G'_M(\gamma_0)$ and $G'_L(\gamma_0)$ to each other at every γ_0 (using the intracycle stiffening index S [18]) and also consider each as a function of γ_0. We calculated these measures of elastic nonlinearity by fast Fourier transform (FFT) methods on the time-resolved strain $\gamma(t)$ and stress $\tau(t)$ signals at each amplitude as described in Sec. V B.

Finally, on distinct samples not already subjected to LAOS, we applied steady uniaxial

strain

$$\epsilon = \frac{l - L}{L} \tag{4}$$

where l is the deformed height of the sample controlled by changes in the rheometer gap, initially at height L. Compression or extension was applied in seven linearly spaced steps between 0% and ±12% ($\epsilon < 0$ in compression and $\epsilon > 0$ in extension). We calculated the uniaxial stress in a sample of radius $a = 0.6$ as

$$\sigma_N = \frac{F_N}{\pi a^2} \tag{5}$$

where F_N is the rheometer reported normal force exerted on the top plate. We superposed an oscillatory shear of $\gamma_0 = 0.05\%$ and $\omega = \pi$ s^{-1} to measure the shear storage modulus G' as a function of uniaxial strain ϵ. Since ϵ was constant within a step, we waited until σ_N and G' relaxed to apply the next 2% gap change, averaging the last four time points of both to compute values for each ϵ. We calculated uniaxial moduli for distinctly oriented samples $\hat{n}_1$ and $\hat{n}_2$ in each species as the slope of linear fits to plots of uniaxial stress vs. uniaxial strain, and denoted them E_1 and E_2. Comparing these as well as G' measured at $\epsilon = 0$ for each orientation, $(G'_0)_1$ and $(G'_0)_2$, allowed us to make general statements about mechanical symmetries in living sponges.

C. Dissection Microscopy

After rheology, samples were removed from the rheometer, put back into artificial seawater, and allowed to rest. We blotted each of excess water, determined its wet mass m_w, and in between four layers of paper towel applied firm pressure ($\sigma_N \sim 1$ MPa), until water could no longer be drawn into fresh, layered paper towel. This method may not remove water bound tightly to protein, but provides an adequate estimate of the mass fraction of bulk water in the tissue $\phi_w = \frac{m_w - m_d}{m_w}$ where m_d is the squeeze-dried mass of the disk.

To characterize sponge skeletal architecture, we submerged individuals of each species in DI water, causing cells to osmotically burst, and agitated gently in several washes of additional DI water to remove remaining cellular debris. Some of the species left behind stiff, fibrous skeletons after washing, while others fully disintegrated in this treatment. Intact skeletons were dried in air before being sampled into disks of distinct orientations $\hat{n}_1$ and $\hat{n}_2$ as in Sec. II A. We imaged these with a USB microscope (Dino-Lite AM4113T) and a

stereomicroscope (Nikon SMZ800). We used the ImageJ (v1.53e) plugin FibrilTool to check for structural anisotropy in the skeletons at this mesoscopic scale (0.001–10 cm). FibrilTool uses a local nematic order tensor as a measure of average fiber orientation, and thus quantifies fibrillar anisotropy within a region of interest (ROI) [21]. We drew three ROIs in each image to determine whether fiber orientation depended on its position within an image or overall tissue disk orientation.

To quantify spicule content in the sponges, we first made 5 mm-diameter tissue cores with a biopsy device. Thin (∼2 mm) core slices were placed in individual wells of a 24-well culture plate with 1 mL of 6% bleach to dissolve all organic material including the protein skeleton while preserving any siliceous spicules (Fig. S6). After dissolution of tissue, the supernatant was removed with care to leave settled spicules undisturbed. We then washed the spicules three times with 1 mL of DI water, allowing them to settle before removing the wash fluid and rinsing a final time with 95% ethanol. A few drops of well-mixed solution were drawn into clean, large-bore pipettes and held vertically for about 30 seconds to allow sedimentation. A single drop (∼0.05 mL) of this sedimented aliquot was then placed on a slide and examined by light microscopy. We used the multipoint tool in ImageJ to count all whole spicules in a field of view to estimate the number density of spicules in different species.

III. RESULTS

A. Mechanics

These eight species (Fig. 1) span six orders within the largest sponge class (Demospongiae) and display an array of growth forms [22, 23]. In five of them, *A. fulva*, *Callyspongia sp.*, *A. polycapella*, *T. keyensis*, and *C. apion* (Fig. 1A,D,E,F,H), we obtained samples perpendicular $\hat{n}_1$, and parallel $\hat{n}_2$, to the assumed substrate and ambient, free-stream flow v (Fig. 1I). Due to various features of their biology, the other three species (Fig. 1B,C,G) required a slightly different sampling strategy as follows. *C. celata* tissue was dense with embedded tracts of sand (Fig. S4C), which resulted in randomly oriented samples $\hat{n}_{\blacksquare}$, $\hat{n}_{\blacksquare}$, and so on. *I. notabilis* was comparatively homogeneous but soft and collapsible upon attempted slicing (Fig. S4D), so we used any mechanically stable and geometrically suitable

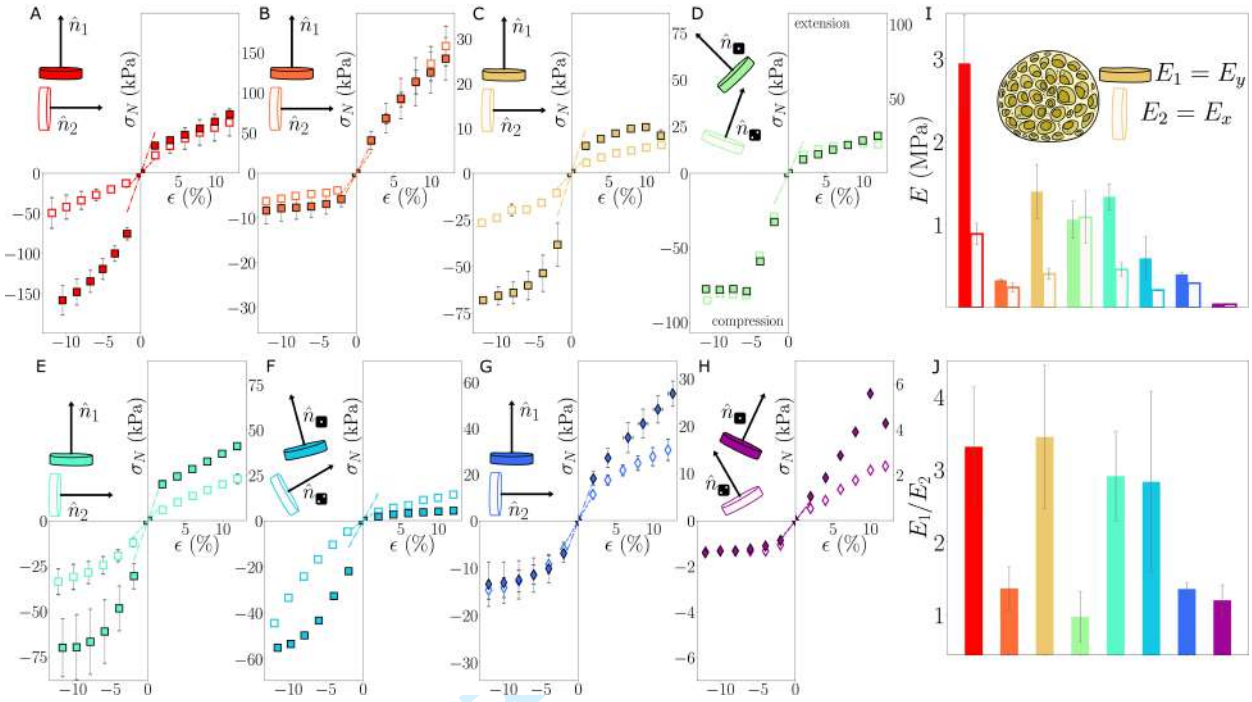

FIG. 3. Uniaxial stress-strain curves for distinct sample orientations $\hat{n}_1$ and $\hat{n}_2$ (filled and unfilled markers) in each sponge. Error bars are s.e. of N samples in A)-C), E), and G) while D), F), and H) have no error bars since in these species we compared pairwise, randomly oriented samples. I) Uniaxial modulus E in MPa J) Ratio of E measured along each direction, E_1/E_2.

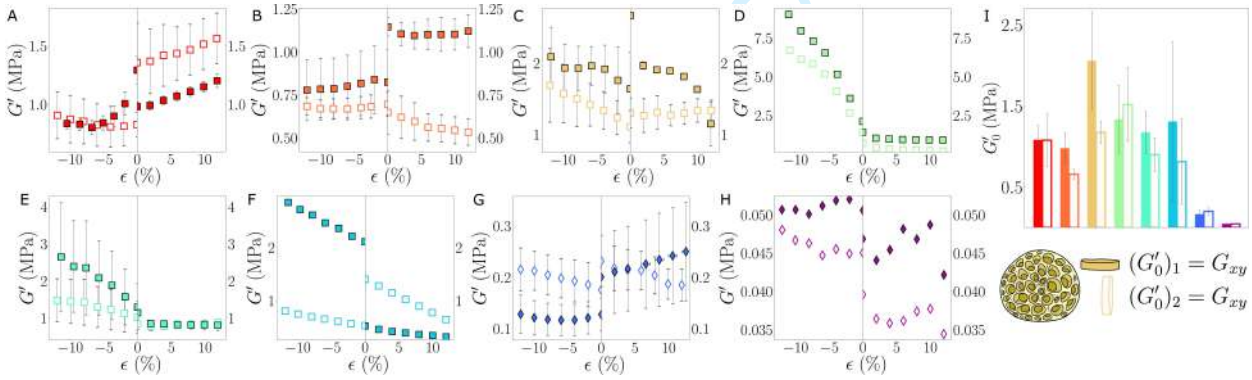

FIG. 4. Linear shear storage modulus G' vs. uniaxial strain ϵ. I) G' at $\epsilon = 0$, G'_0.

samples (Fig. 1C inset) while making note of distinct orientations. *Tethya sp.* had a stiff cortex that overloaded the rheometer's normal force transducer ($F_N > 50$ N), barring us from rheology on the outer part of this sponge (Fig. S4A). Its pith was softer but brittle with long and flexible spicules, resulting in randomly oriented samples for *Tethya sp.*

Sampling geometries and uniaxial stress-strain curves in each species of sponge are shown

in Fig. 3A-H. We took slopes within the linear regime of each as an effective, uniaxial modulus $E = \sigma_N/\epsilon$ (Fig. 3I). The uniaxial mechanics of *A. polycapella*, *C. apion*, *T. keyensis*, and *Tethya sp.* uniaxial mechanics were highly dependent on sample orientation. Their tissue more strongly resisted compression along the $\hat{n}_1$, than along the $\hat{n}_2$ direction. *C. celata* curves on the other hand, were independent of sample orientation but highly nonlinear, sharply plateauing in σ_N at $\epsilon = -6\%$. The ratio of uniaxial moduli measured along each direction, E_1/E_2, confirms the former sponges were about three times stiffer along $\hat{n}_1$ compared with $\hat{n}_2$ (Fig. 3J). By contrast, this ratio's for *Callyspongia sp.*, *A. fulva*, and *I. notabilis*, was closer to unity were much less different along different directions ($E_1/E_2 = 1.3$), a result suggesting the tissue of these three sponges contains at least one plane of isotropic isotropy. The E_1/E_2 ratio in *C. celata* was equal to one, and therefore we conclude *C. celata* was the closest to isotropic of the sponges tested.

The shear storage modulus G' (measured at $\omega = \pi$ s^{-1} and $\gamma_0 = 0.05\%$) as a function of uniaxial strain ϵ is shown in Fig. 4. It increased with compression in *C. apion*, *C. celata*, *T. keyensis*, and *Tethya sp.*. Instead, in *A. polycapella*, *Callyspongia sp.*, *A. fulva*, and *I. notabilis*, G' stiffened modestly in compression, and only after initially softening. Reconstituted networks of collagen and fibrin have also been shown to compression soften, while whole tissues made of these biopolymers plus cells, compression stiffen [24]. We found that sponge tissue with living cells can do either, does both depending on the species. This suggests that the presence of deformable but volume-conserving cells [25], is not the biggest contributor to compression stiffening in sponges.

In Fig. 5, we compare sponge multiaxial mechanics with those that of mammalian tissues. G' as a function of compressive stress $|\sigma_N|$ in brain [26], liver [27], and adipose [28], is approximately linear, $G'(\sigma_N) = m|\sigma_N| + G'_0$ with slopes $m \leq 1$ [29]. The sponges compression stiffen linearly as well, but had $m >> 1$, with m highest in *C. celata* at about 60 (zoomed inset). *C. celata* also displayed a sharp discontinuity at $\epsilon = -6\%$, where m goes to infinity and G' increases to 9 MPa, more than four times its initial value at $\epsilon = 0\%$. By complete contrast, *A. polycapella*, *Callyspongia sp.*, and the spicule-less sponges, change their G' relatively little with $|\sigma_N|$, indicating low multiaxial responsivity.

In Fig. 5B, we normalize the change in G' by G'_0, and see that under the significantly smaller strains we applied ($\epsilon = -12\%$ vs. $\epsilon = -40\%$ in brain [26], for example), sponges overall accessed a larger scaled range of G' for every scaled increment of $|\sigma_N|$, than did any of the mammalian tissues. The slope produced by this approximately linear scaling also compared to cite

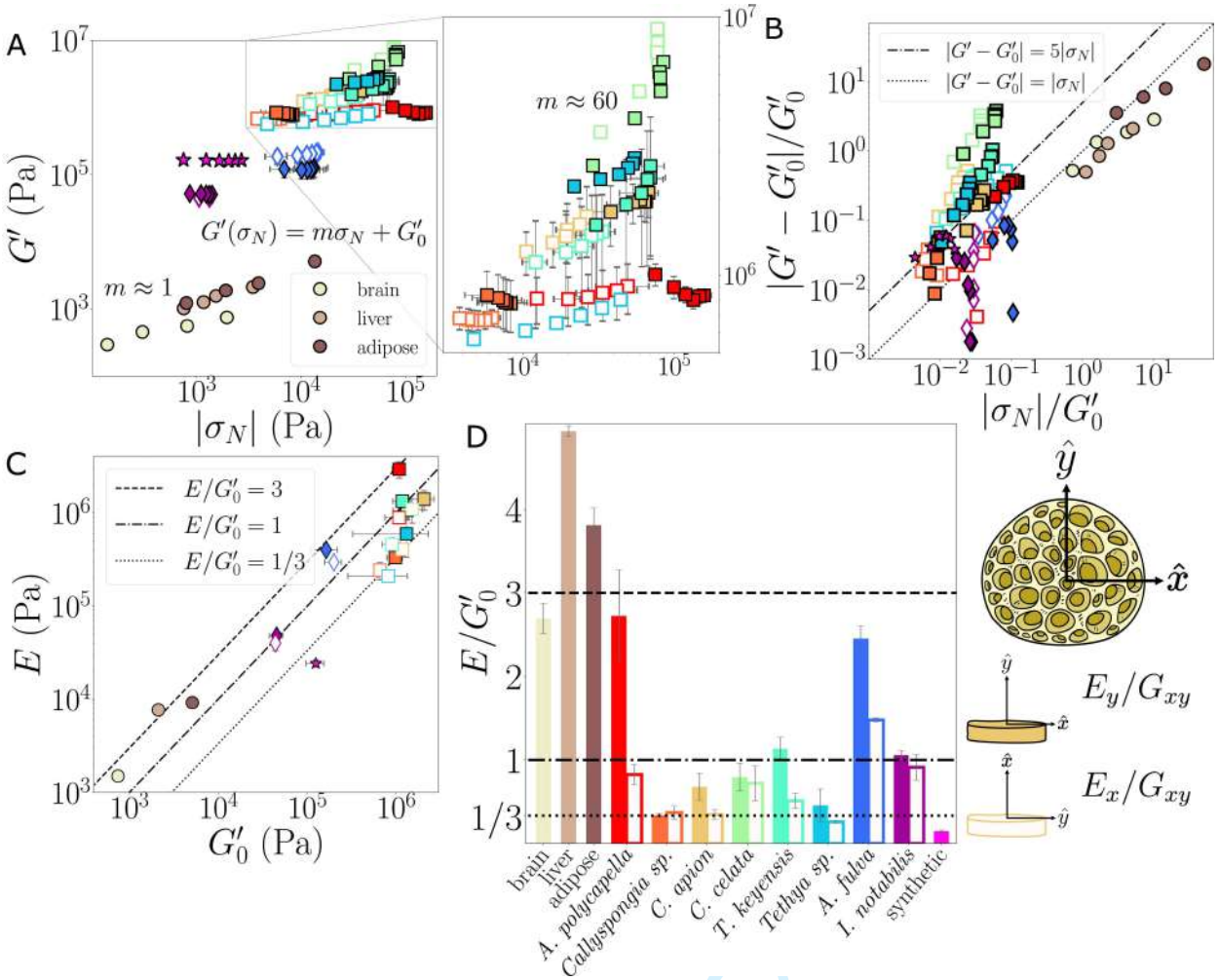

FIG. 5. A) G' vs. the magnitude of compressive stress $|\sigma_N|$ in the sponges and mammalian brain, liver, and adipose tissue [26, 27, 28]. B) Change in magnitude of G' vs. corresponding change in $|\sigma_N|$, both normalized by G'_0. C) E vs. G'_0 along each direction in the sponges and in the mammalian tissues. D) E/G'_0 bar plot; the diagram adjacent depicts which uniaxial and shear moduli were measured in the rheometer based on the sampling geometry.

gives an estimate of the persistence length (bending rigidity [30, 31]) of the biopolymers underlying these living tissues. We found the mammalian tissues at a scaling of about one (dotted line), and the sponges varied from one ~~through~~ to five (a value typically used *in silico* and found in semi-flexible biopolymer gels ([31], dashed-dotted line) and upwards. This indicates ~~a comparatively large~~ both a range of bending rigidities in the spongins that make up the tissue of these species, and also suggests a smaller average polymer bending rigidity, given that larger slopes translate to smaller bending rigidities [31]. Overall, most of the sponges had larger slopes than one, and therefore spiculated spongins

Is this sentence implying that spongins are stiffer locally, but also of higher molecular weight than mammalian collagens, leading to lower per-polymer bending rigidity? If so, say that directly, it is unclear here and potentialy interesting.

are more flexible than mammalian collagens but locally quite stiff. Taken together, these results suggest that spiculated spongins may be semi-flexible polymers.

We compare E with G_0' in the sponges and mammalian tissues in Fig. 5C. Material constants in sponges would be most accurately determined from constitutive models that include dissipation both from fluid flow within the pore space [32] and viscoelastic flow (Sec. III B) of the solid constituents, the spiculated spongins. Here, the diversity in the measured linear elastic constants E and G_0' is sufficient for comparative biology among this set of sponges, and ~~vs~~ to brain, liver, and adipose tissue. Interestingly, E was larger than G_0' in all of the mammalian tissues, while the opposite was true in most of the sponges (Fig. 5D). These data recapitulate that mammalian tissues are incompressible (like rubber, with Poisson's ratio $\nu = 1/2$ [27]), while the sponges approach what is expected for extremely compressible materials, $\nu = -1$ [33]. Negative values of ν imply auxeticity, or the tendency to contract instead of bulge transversely when compressed, and 'spongy' materials like re-entrant polymer foams and many honeycomb structures are auxetic [34]. Through the usual constraints associated with the stress and strain tensors of linear elasticity (Sec. V A), we found ν ~~take on~~ to occupy negative values in all of the sponges (Tab. S1), suggesting auxeticity is possible in Poriferan body tissue.

B. Linear Viscoelasticity

The linear viscoelastic response of sponge tissue as a function of driving frequency ω is shown in Fig. 6. The storage modulus $G'(\omega)$ was an order of magnitude larger than the loss modulus $G''(\omega)$ and spanned two orders of magnitude ($10^4 - 10^6$ Pa) in these sponge species. Sponges with spicules (squares) were an order of magnitude stiffer than those without (diamonds). $G'(\omega)$ followed a very weak power-law in all specimens, including the synthetic cellulose sponge, but interestingly, $G''(\omega)$ also followed a frequency power-law for the synthetic sponge only, and was non-monotonic and disparate among living sponges (Fig. 6B).

The ratio of dissipated to stored energy in the tissue when sheared, $\tan\delta$, highlights these disparities (Fig. 6C). In *C. apion*, *C. celata*, *Tectitethya sp.*, and *Tethya sp.*, $\tan\delta$ decreases at low ω, followed by a slow increase in some, or a plateau in others. *A. polycapella*, *Callyspongia sp.*, and *I. notabilis* behave similarly, but $\tan\delta$ takes values roughly four-fold

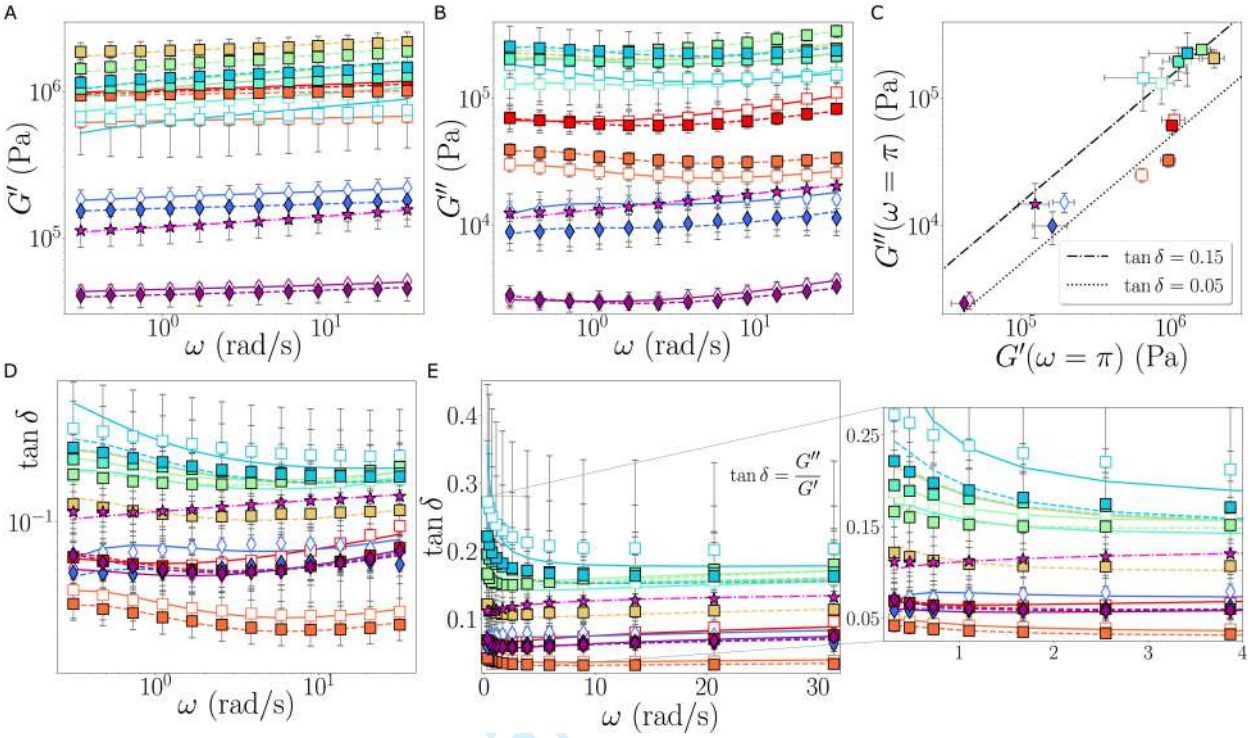

FIG. 6. Sponge tissue frequency sweeps at $\gamma_0 = 0.05\%$. A) $G'(\omega)$ B) $G''(\omega)$ C) G'' vs. G' at $\omega = \pi$ s^{-1} D) $\tan\delta$ vs. ω, replotted on linear axes in E). Curves are fits of the fractional solid model [16] and error bars are mean±s.e. of N samples.

smaller (Fig. 6D). In other words, the first group of sponges dissipate four times as much energy when sheared compared to the second group, and many of the sponges had dissipation minima at specific frequencies (Fig. 6E).

None of the classical viscoelastic circuit models that we fit provided adequate descriptions of $G'(\omega)$ and $G''(\omega)$ (Fig. S8). We also fit a model including a fractional element that reproduces the power-law behavior associated with a continuous distribution of relaxation times in biological materials [16]. This model reproduced the power-law storage behavior and the non-monotonicity of dissipation in the live sponges with high accuracy.

C. Nonlinear Viscoelasticity

For increasing amplitude of oscillatory shear strain γ_0 (LAOS), sponge tissue responded nonlinearly by softening as indicated by decrease of $G'_M(\gamma_0)$ and $G'_L(\gamma_0)$ (Fig. 7A-C), defined in Sec. II B. We let the onset of softening γ_a (dotted vertical lines) be where G'_M first

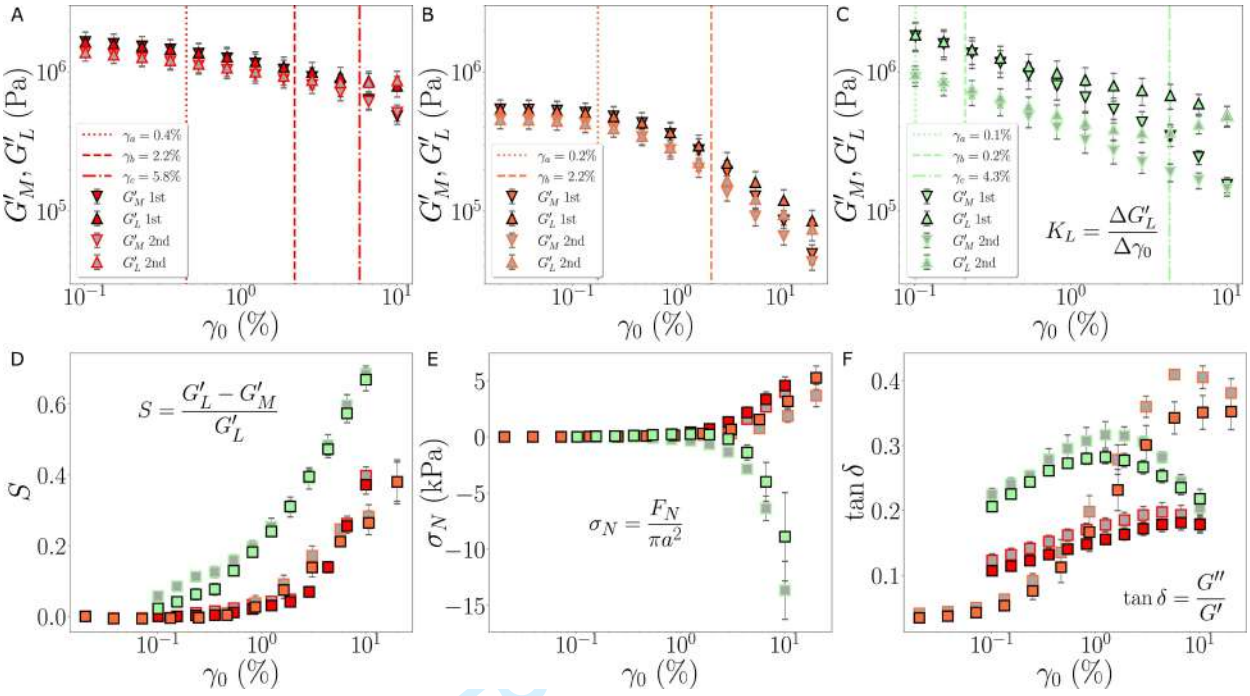

FIG. 7. Sponge tissue amplitude sweeps at $\omega = 4\pi$ s^{-1}. G'_M (downward triangles) and G'_L (upward triangles) vs. γ_0 in A) *A. polycapella* B) *Callyspongia sp.* and C) *C. celata*. Data for the second round are in gray. D) S E) σ_N F) $\tan\delta$ vs. γ_0

decreased more than 10% from its previous value. *C. celata* began softening at a smaller γ_a and also softened more than *A. polycapella* and *Callyspongia sp.* over the course of one LAOS test. By the final amplitude, G'_M had decreased by roughly 90% in *C. celata* (Tab. S2).

Intriguingly, *A. polycapella* and *C. celata* tissue had additional shear nonlinearities arise after pre-conditioning of the first LAOS test. During the second LAOS test, the large strain elastic modulus $G'_L(\gamma_0)$ (gray upward triangles) in these two species increases after another strain γ_c (dashed-dotted vertical lines). This was most pronounced in *C. celata* (Fig. 7C). It softened so much in the first LAOS but still returns exactly to its state at the end of the first LAOS, indicating strong shear softening followed by equally strong stiffening. In other words, $G'_L(\gamma_0)$ has an inflection point during the second LAOS in these species. *Callyspongia sp.* does not, despite it being sheared ~~to a twice larger~~ to twice the value of $\gamma_0 = 20\%$. We ~~made~~ set γ_c be ~~where~~ to the point at which the numerical derivative $K_L = \Delta G'_L / \Delta\gamma_0$ changed sign to confirm there was no inflection point in $G'_L(\gamma_0)$ for *Callyspongia sp.* during the second round of LAOS (Tab. S3).

This needs a rewrite - reads like it is being said out loud for the first time and I'm not sure what it is trying to say.

The time-resolved trajectory of the shear stress $\tau(t)$ ((ii) Fig. S2) in response to oscillating shear strain $\gamma(t)$ ((i) Fig. S2) reveals further richness in the larger strain viscoelasticity of

sponge tissue. $\tau(t)$ increases nonlinearly during a single cycle from $\gamma = 0$ to $\gamma = \pm\gamma_0$ as indicated by concave-up parametric plots of $\tau(t)$ vs. $\gamma(t)$ (L-B curves Fig. S2(iv)). We evaluated this stiffening at each γ_0 with the index $S = \frac{G'_L - G'_M}{G'_L}$ and ~~made~~ set its onset γ_b ~~be where~~ to the point at which $S \geq 0.1$ [18]. $S = 0$ signifies no stiffening within a cycle and elliptical L-B curves with well-defined semi-major and semi-minor axes (L-B curve lower insets). The more positive is S, the greater G'_L compared with G'_M, the more upwardly concave the L-B curve, and the greater the stiffening (L-B curve upper insets) at ~~that~~ the given γ_0. This stiffening nonlinearity occurs during a single oscillation from $\gamma = 0$ to $\gamma = \pm\gamma_0$ for $\gamma_0 > \gamma_b$.

The onset of stiffening γ_b (dashed vertical lines) followed the same trend as γ_a. It was about ten times smaller in *C. celata* compared with *A. polycapella* and *Callyspongia sp.* (Tab. S2). In other words $\gamma_{a,b}^{Cliona} < \gamma_{a,b}^{Callyspongia} < \gamma_{a,b}^{Axinella}$ was true. S increased monotonically with increasing γ_0 in all species and by $\gamma_0 = 10\%$ *C. celata* had the largest and *Callyspongia sp.* the smallest S (Fig. 7D). *C. celata* shear stiffened more (more positive S) and after smaller strains than *A. polycapella* and *Callyspongia sp.* when $\gamma(t)$ is increased over the trajectory of a single cycle but also softens more (more negative K_L) and at smaller strains (Tab. S2).

C. celata was also distinct from *A. polycapella* and *Callyspongia sp.* by the sign of its induced normal stress and ratio of dissipation to storage as functions of γ_0 (Fig. 7E,F). Due to perpendicular expansion upon shearing, positive normal stress is induced in many materials [35]. Semi-flexible biopolymer networks instead pull downward when sheared, exhibiting negative normal stress [35]. Surprisingly, sponge tissue did both: *A. polycapella* and *Callyspongia sp.* pushed upward on the top plate with a positive normal stress of roughly 5 kPa while *C. celata* pulled downward with negative normal stress twice as large by $\gamma_0 = 10\%$. Finally, $\tan\delta$ increases with γ_0 in all three species initially, but *C. celata* reaches a clear maximum dissipation (Fig. 7F). *A. polycapella* and *Callyspongia sp.* begin the LAOS experiment about half as dissipative as *C. celata*, and after increasing initially, dissipation then only marginally decreases for *A. polycapella* and *Callyspongia sp.* over this physiological range of γ_0.

D. Morphological & Skeletal Characteristics

As described in Sec. II C, we imaged mesoscopic features in the washed fibrous skeletons of less dense sponges (Fig. 8). *A. fulva* grows as rope-like branches that hang downward. It has no spicules but a relatively stiff spongin skeleton of irregular polygons with large mesh sizes of a few millimeters. We could not distinguish $\hat{n}_1$ from $\hat{n}_2$ in *A. fulva* samples at this scale. *I. notabilis*, the other sponge without spicules in our dataset, has a similar skeleton (Fig. S5B) and a lobe-like, branching growth form. *Callyspongia sp.* has hollow tissue (Fig. 8H), making it ultimately vase-like, but when viewed on a smaller scale by stereomicroscope (Fig. S5F,G) its tissue looks like that of *A. fulva* and *I. notabilis*.

By contrast, *A. polycapella* is conspicuously solid and axially arranged. This sponge forms erect, tree-like structures (Fig. S3), with one central column, or trunk. Fig. 8E (F) shows an $\hat{n}_1$ ($\hat{n}_2$) disk of *A. polycapella*. The red lines signifying local nematic order and thus average fiber orientation show a condensed region of axial fibers, a trait well-documented in erect sponges [36, 37], as well as radial and tangential fibers. *Tethya sp.* and *T. keyensis* growth forms are radially symmetric but the nematic tensors drawn with FibrilTool also reveal three principal fiber directions as in *A. polycapella* (Fig. S4A,B). Materials such as wood [38], bone [39], and brick [40], also have three principal directions and are thus orthotropic. A point within an orthotropic material has three mutually perpendicular planes of reflection symmetry [39] and material properties are different along each principal direction. This was most obvious in *A. polycapella*, whose tissue does bear a striking resemblance to a tree trunk (Fig. S5D), but we also found structural and mechanical signatures of orthotropy in *T. keyensis* and *Tethya sp.*

In terms of the bulk density measured by the mass fraction of water ϕ_w in their tissue, *C. apion*, *C. celata*, *T. keyensis*, and *Tethya sp.* were significantly denser ($\phi_w \leq 0.5$) than *A. polycapella*, *Callyspongia sp.*, *A. fulva*, and *I. notabilis* ($\phi_w \geq 0.7$) (Fig. 9A). Multiplying the mass fraction of solids $\phi_s = 1 - \phi_w$ by the total density of the sponge tissue disk m_w/V, gives an estimate of the concentration of spongins c. On a log-log plot of G_0' vs. c in mg/mL, we find an approximate scaling of $G_0' \sim c^{11/5}$ to fit the sponge data (Fig. 9B). This agrees with previous results for the dependence of the network shear modulus on semi-flexible polymer concentration [41], providing further evidence for general semi-flexibility of spiculated spongins.

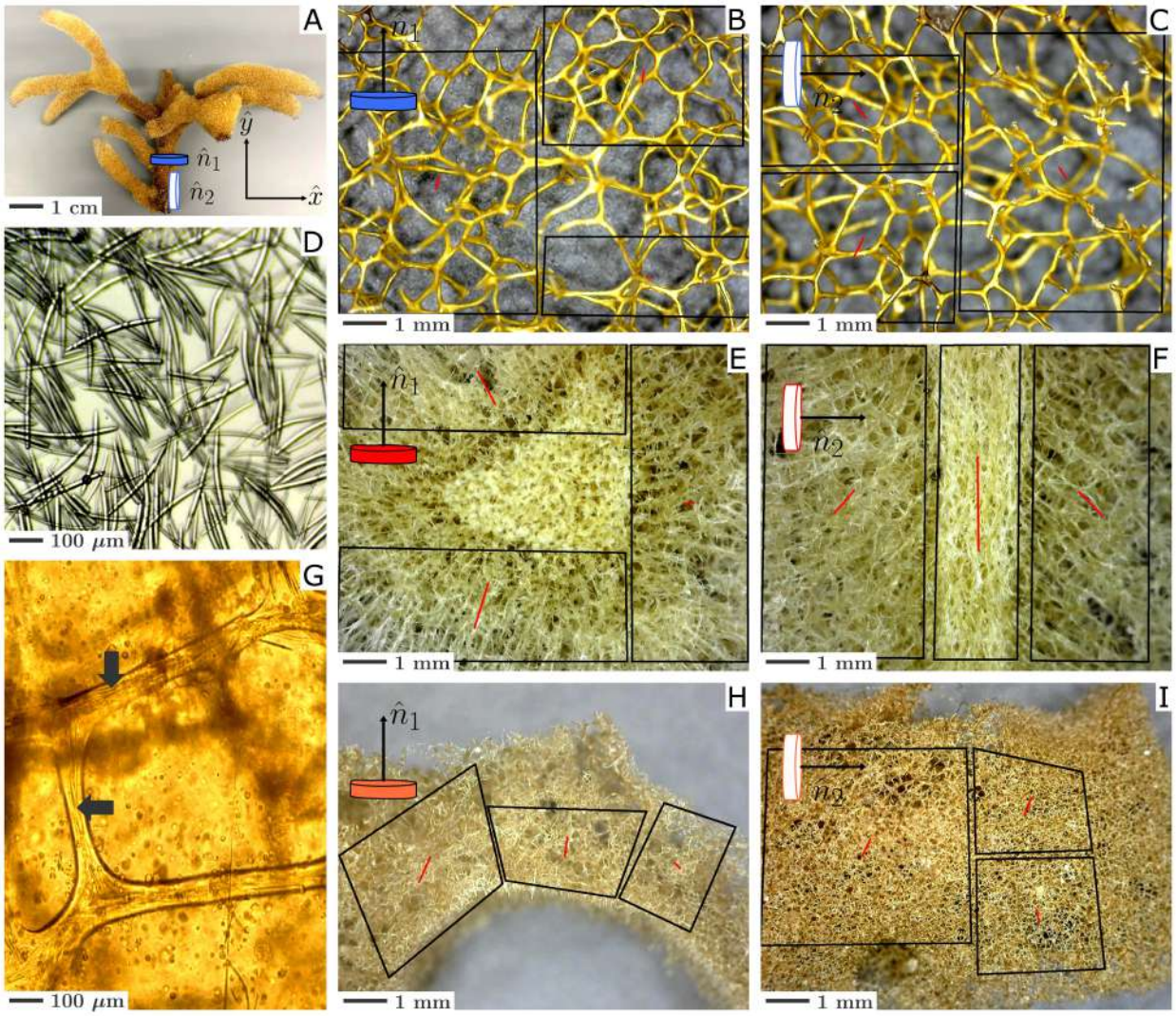

FIG. 8. Sponge structure and morphology. A) dried *A. fulva* spongin fiber skeleton sampled into B) $\hat{n}_1$ and C) $\hat{n}_2$ disks. Red lines inside black boxes correspond to average fiber orientation measured using FibrilTool [21]. D) *A. polycapella* spicule preparation. E) $\hat{n}_1$ F) $\hat{n}_2$ *A. polycapella*. G) *Callyspongia sp.* skeleton, arrows show spicules confined inside spongin fibers. H) $\hat{n}_1$ I) $\hat{n}_2$ *Callyspongia sp.*

The major component of the spicule population in these species were monactine (Fig. S7). *Tethya sp.* (Fig. S7D) also contained spiky spherical spicules (spherasters) in its cortex only. We did not count these since they were much more numerous than the monactine strongyloxeas found in both the cortex and pith. *A. polycapella* oxeas (Fig. 8D), *Callyspongia sp.* oxeas (Fig. 8G), and *C. celata* tylostyles (Fig. S7B) were similar in size and shape: monactine and about 100 μm long and 10 μm thick, though arranged differently with respect

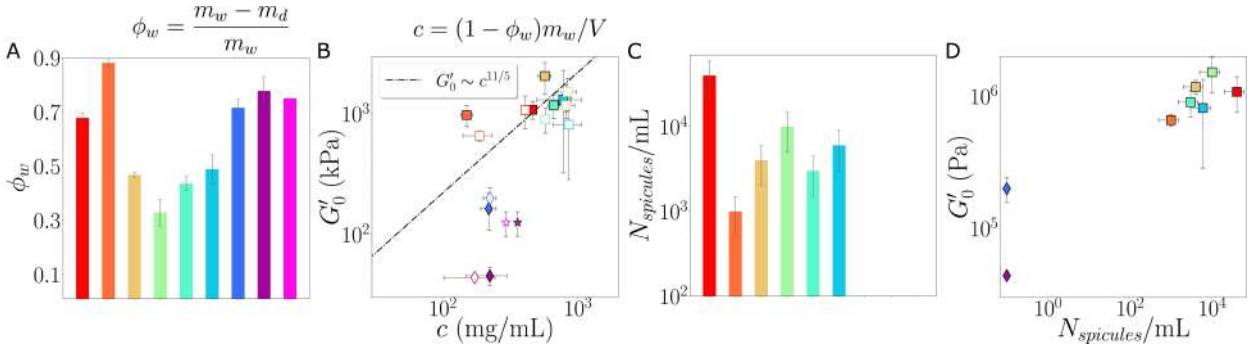

FIG. 9. A) mean mass fraction of water $\phi_w \pm$s.e. of N disks B) G_0' vs. the concentration of spongins c estimated from ϕ_w. C) estimated number of spicules per mL of tissue $\pm 50\%$. D) G_0' vs. the number density of spicules.

to the softer part of the tissue. The three fiber directions in *A. polycapella* are spicule-reinforced [42] while spicules in *Callyspongia sp.* are constrained entirely within the fibers of its spongin network [43]. *C. celata* spicules are arranged and oriented densely and randomly [22], along with a surprising amount of sand (Fig. S6F). We observed *A. polycapella*, *C. apion*, *C. celata*, *T. keyensis*, and *Tethya sp.* tissue dissolve slowly and vigorously in bleach (Vid. S1) and produce strong light scattering in culture wells (Fig. S6). These observations and our estimates of spicule number density (Fig. 9C-D) confirm heavier spiculation in these sponges compared with *Callyspongia sp.* and the two species without spicules.

IV. DISCUSSION

We explored the mechanics and dynamics of a set of sponge species using rheology and microscopy. Our results ~~on the detailed and surprisingly diverse~~ show a surprisingly detailed and diverse tissue mechanics ~~of these sponges informs~~ informing our understanding of the great diversity of body forms both within and between species in this phylum.

We first consider the species in our dataset with the most pronounced axial skeleton and erect growth form, *A. polycapella*. An axial skeleton is not unique to *A. polycapella* but present across many sponge clades and thought to be a morphological mechanism that generates rigidity [36, 37, 44]. Despite possession of this trait, *A. polycapella* had a smaller stiffness, i.e. shear rigidity G_0', than *C. celata*. The sand that *C. celata* incorporated in addition to its spicules must be increasing its G_0'. Since the presence of spicules at all

increased G_0' by a factor of ten, stiffness is proportional to the total volume fraction of stiff inclusions, including sand grains. We speculate that the cortex of *Tethya sp.* overloaded the normal force transducer because spheraster-form spicules led to jamming in the physical sense, where in a system with sterically repulsive interactions, density and geometry combine to prohibit translational motions [45]. The dense, sandy inclusions in *C. celata* may have caused jamming in some regions of its tissue. So, while axial skeletons do not appear to cause anomalously high G_0', or stiffness, ~~in our dataset~~, the presence of an axial skeleton does evidently produce orthotropic elasticity. Orthotropic elasticity is when the material stiffness at a particular point in a body differs along three mutually orthogonal axes.

This form of anisotropic stiffness likely contributes to the ability of erect sponges to withstand pressure drag experienced in free stream, steady flow v (Fig. 1I). The magnitude of this drag force is

$$F_D = \frac{C_D \mathcal{S}}{2} \rho v^2 \tag{6}$$

where C_D is the drag coefficient, $\mathcal{S}$ is the area exposed to flow, and ρ is the fluid density [46]. We consider *A. polycapella* as an upright, solid cylinder of radius a and length ℓ (Fig. 1E) and therefore $\mathcal{S} = 2a\ell$. C_D depends on the Reynolds number $Re = \rho v \ell / \eta$ where η is the fluid viscosity. Using the range of v from Sec. II B and values of ρ and η for seawater at 20 degrees C, we find $10^2 \lesssim Re \lesssim 10^5$ over which $C_D \approx 1$ for a cylinder [46]. The maximum flow-induced shear stress may be estimated as $\tau_0 = F_D / \pi a^2$ and thus written as a function of v using Eqn. 6

$$\tau_0 = \frac{C_D \ell}{\pi a} \rho v^2 \tag{7}$$

This equation states that the more slender a cylindrical sponge is through ℓ/a the larger is τ_0. The Loop Current [47], which runs through places where *A. polycapella* is common along the Gulf of Mexico, around Florida, and up into northern Atlantic waters [48], can reach $v = 80$ cm/s and would impart $\tau_0 \approx 4.2$ kPa. As *A. polycapella* and other tree-like sponges grow taller, orthotropic tissue that is stiffest along $\hat{y}$ is necessary to withstand large τ_0. Wood, another orthotropic material [38] that is stiffest along its central axis, is also subjected to a single principal force: wind-induced drag [46]. Sponges with axial skeletons are therefore mechanically analogous to trees by this reasoning, ~~and using them for reef dendrochronology should be possible in principle. The tangential fibers of *A. polycapella* (Fig. 8F) correspond to surfaces of earlier accretive growth, as they do in a tree's trunk.~~

There are a whole lot of ideas in this paper, I think this one is just making it harder to follow your larger message.

Eqn. 7 also shows that as ℓ increases during growth, sponges could keep the load on themselves constant by keeping the ratio ℓ/a constant, which would fix the value of the tissue stiffness $G_0' = \tau_0/\gamma_0$ in each branch and across the whole animal. This line of reasoning suggests global rigidity [49], as mediated by ℓ/a, is the tissue network parameter optimized by sponges with axial skeletons [50]. This model in turn predicts that sponges should branch in a self-similar or fractal way, with fractal dimension increasing in areas of higher flow speed in order to share a larger load on the tissue τ_0 between more branches. In other words, the cost of construction of new branches is fixed throughout the whole height of the animal. Tree-like sponges do branch in a self-similar way [50, 51], with higher fractal dimension measured in individuals from sites of higher flow v, but relevant optimization functionals have not been explored like they have in more familiar transport networks [52].

In contrast, our results suggest that *T. keyensis* and *Tethya sp.* tissue is orthotropic but these sponges are not obviously tree-like since they do not form branches. They are erect, though, and thus exposed to one principal force: pressure drag which acts perpendicular to $\hat{y}$. Indeed, dissecting them revealed thicker skeletal fibers parallel to $\hat{y}$ than along $\hat{x}$ or $\hat{z}$ (Fig. S4A,B). Given the above, it is likely that axial and radial sponge skeletons are both orthotropic. The former grows cylindrically while the latter spherically, but sometimes within a single individual, both types exist (Fig. 9 in [53]), lending support to the idea that each is a manifestation of orthotropy. As long as a sponge is slender enough ($\ell \gtrsim a$) such that flow separates around it [54], its tissue must be stiffest along $\hat{y}$ to withstand this. For low-aspect-ratio sponges ($\ell < a$), Eqn. 7 no longer holds as such shapes are subject to different forces.

In addition to pressure drag, there will be other flow-induced forces on low-aspect-ratio sponges like 'skin' or viscous drag, lift, and accelerating flows. The calculation of these is subtle and presented in [9, 54], so we do not include it here. However, the key point is that both kinds of drag, lift, and accelerating flows can all become important in different dynamic flow conditions, and thus the direction of the net force on a low-aspect-ratio sessile animal is not generally perpendicular to $\hat{y}$ or even fixed. It then makes sense for an amorphous, massively encrusting sponge like *C. celata* to have isotropic tissue, since it contends with applied forces that are time-dependent, and from multiple directions. *Callyspongia sp.*, *A. fulva*, and *I. notabilis* tissue was also more isotropic, but these sponges form hollow cavities, making them vase-like and mechanically transversely isotropic, i.e. the xz-plane is one of

isotropy and is transverse to the y-axis of symmetry, the long axis of the vase [39]. In other words, the body cavity, or spongocoel, is an axis of mechanical symmetry that is typically perpendicular to the substrate plane in vase-like sponges. Sponges of different growth forms are therefore well-adapted to the same environments through unique tissue mechanical strategies. Moreover, it has been shown that high-aspect-ratio forms like erect cylinders, encounter primarily fine particles whereas low-aspect-ratio forms encounter larger particles [54]. This sedimentation gradient would enable sponges of different growth forms to specialize in differently-sized food particles.

In many ways, *C. celata* had the richest rheology of the sponges we tested. Its tissue appeared to undergo a compression-induced phase transition as indicated by the discontinuity in G' vs. $|\sigma_N|$. Recently, simulations have shown that networks of semi-flexible polymers embedded with stiff inclusions can undergo a phase transition as the inclusions rearrange non-uniformly (non-affinely) under bulk compression [55]. Our multiaxial mechanical data was qualitatively very similar to these simulations. The slope change at $\epsilon = -6\%$ in *C. celata* and others may be seen as the signal of imminent jamming. Rearrangement of stiff inclusions during compression induces local tension within intrinsically semi-flexible biopolymers [56], leading to macroscopic increase of rigidity [55]. Semi-flexible polymers are those which are flexible on scales larger than their persistence length [30], but locally quite stiff, and nonetheless subject to thermal fluctuations. Many ubiquitous biopolymers are semi-flexible [57]. Our mechanical data, taken together with the biochemical similarity of spongins to fibrillar and non-fibrillar mammalian collagens [58, 59], and the fact that the average spongin fibril size (10 nm [5]) is comparable to intermediate filament sizes [57], points to spongin semi-flexibility. In other words, spiculated spongin bundles likely contribute significant stretching, but also bending energies towards the total energy of deformation of sponge tissue.

The strong compression stiffening in sponges compared with mammalian tissues likely comes from shape constraints as described above, but also volume constraints from cells acting as deformable inclusions [25]. Sponge microenvironments can be dense and crowded, especially in high-microbial-abundance species where symbiotic bacteria in the tissue are $\sim$100 times more numerous than in low-microbial-abundance species [60]. The effects of cell confinement and in turn nuclear deformation during cell motility have only just begun to be explored in mammalian systems [24, 61]. Because of the purported absence of cytoskeletal

intermediate filaments like nuclear lamins in sponges, global compression of tissue may cause contact percolation of sponge cells and subsequent nuclear deformation (Fig. 57A in [5]) and mechanical signaling. For this to be plausible, sponge cells must be able to respond to strains $\lesssim$10%, considering flow-induced forces would have to be transmitted from the surrounding tissue.

The observed auxeticity of sponge tissue provides a possible mechanism for amplification of strain in biological systems [34]. While we made indirect measurements of Poisson's ratios ν_{ij} in this set of sponges (Tab. S1), direct observation of contraction upon compression of a randomly picked marine sponge (Vid. S3) confirms ν generally takes negative values in these animals. To our knowledge, there are no examples of bulk collageneous mammalian tissues which are auxetic. Auxetic re-entrant polymer foams (Fig. 2 in [62]) ~~certainly~~ bear a resemblance to the fiber skeletons of *Callyspongia sp.*, *A. fulva*, and *I. notabilis*. Since sponges are generally subject to stresses 1–10 kPa and strains rarely above 10%, their cells may be able to respond to these comparatively small mechanical shifts by living within auxetic tissues which amplify applied strain by avoiding changes of dimension. Some models of auxetic response show that the walls of the voids within the material collapse inward in controlled fashion [33]. Local strain at these points is presumably very high, and a potential source of a cellular mechanobiological response.

Our results on the nonlinear viscoelasticity in sponges point at general responsiveness of sponge tissue to comparatively small, flow-induced strains. *C. celata* begins shear softening at $\gamma_a \approx 0.1\%$, an onset at least ten times smaller than in collagen gels [20]. In fact, for *in vitro* collagen, the extent of shear softening is weak enough that it is seldom reported on [20], but living sponge tissue softened significantly. The strong softening in *C. celata* might allow structural remodeling in the face of increasing γ_0. *C. celata* and *A. polycapella* shear stiffen at $\gamma_c \approx 5\%$, an onset four times smaller than in collagen gels ($\gamma_c \approx 20\%$ [20]) and they only do so after pre-conditioning with one round of LAOS. During the second round, $G'_L(\gamma_0)$ decreases as before, until γ_c where it begins to increase as described in Sec. III C. We discuss this important subtlety below.

Cyclically loading a large class of disordered systems can allow mechanical memory of steady-state driving amplitudes [63, 64]. Sponge tissue is a ~~great~~ candidate for mechanical memory formation. It is deformable but stable, made of heterogeneous network structures that rearrange under applied strain [65]. We interpret the shear stiffening only after a second

round of LAOS in *A. polycapella* and *C. celata* as a return to a previous rheological steady-state: the final applied strain γ_0 and stress response τ_0 (encoded by $G'_M(\gamma_0)$ and $G'_L(\gamma_0)$) from the first round. This effect is also apparent in the L-B curves for these two species (Fig. S2 rows A and C, col iv) and is more obvious in *C. celata*. Considering this species' more granular, disordered nature, it would make sense for its tissue to recall 'training' strains with higher fidelity compared with *A. polycapella*. Furthermore, the general non-monotonicity of dissipation ($\tan\delta$) as functions of both ω and γ_0 in living sponge tissue implies tunability and responsivity [63]. *C. celata* must also be more tunable than any of the other sponges tested, given it had such a clear maximum dissipation at a small γ_0. Since memory formation is intrinsically tied to non-equilibrium dynamics [63], this suggests *C. celata* tissue is more irreversibly driven by flow than *A. polycapella*.

We speculate on the absence of a strain-stiffening nonlinearity (γ_c) in *Callyspongia sp.* by considering how its spicules are constrained within the softer fibers of its tissue. As this sponge is sheared, its spicules presumably slide past each other or perhaps only weakly interact but still inside large spongin fibers (Fig. 8G). Past γ_a, the spicules may rupture out of these fibers, causing the more dramatic softening between $\gamma_a < \gamma_0 < \gamma_b$ (Fig. 7B). This sponge was also the least dense of any we tested, such that there may be too much open space in its tissue for spicules to abut and create internal strain. We assume that γ_b (γ_{intra} in [20]), corresponds to the strain at which nonlinear elastic stiffening [56] of the spiculated spongin part of the tissue becomes relevant. That *A. polycapella* and *Callyspongia sp.* had similar values of $\gamma_b \approx 4\%$) and the same sign of induced normal stress under shear (positive) but $\gamma_b \approx 0.5\%$ in *C. celata*, which had an opposing sign of induced normal stress (negative), suggests major physical differences and diversity in spiculated spongins.

In any case, *C. celata* must have a strong interaction between its softer fibrous network and stiffer spiculated skeleton, and we suggest this sponge and those like it are in the same class of disordered systems as colloidal gels, which have recently been demonstrated to have an ability to embed mechanical memories perpendicular to a driving shear [65]. The large magnitude of the induced negative normal stress in *C. celata* may even be connected to the 'recording' of a high-fidelity memory through compression. It is curious that ~~as a deformation,~~ compression appears more lossy than shear. Overall, increased sensitivity and tunability in disordered tissue, low-aspect-ratio growth form sponges like *C. celata*, could be a trade-off with the stability that mechanical order provides in more durable, higher-aspect-

ratio sponges like *A. polycapella* and *Callyspongia sp.*

ACKNOWLEDGMENTS

We are grateful for Qiuting Zhang's assistance with the rheometer software and the collection of time-resolved LAOS data. We thank Nikhila Kumar for counting spicules in ImageJ. Sponge identification was possible thanks to Eric Lazo-Wasem, senior collections manager in the Invertebrate Zoology Division of Yale Peabody Museum. We are also thankful for photography assistance from Dr. Casey Dunn and constructive discussions on sponges with Jasmine Mah. Finally, we thank Reviewer #2 for helping improve the accuracy of the manuscript. E.A.K. and P.A.J. were supported by the U.S. National Science Foundation (Grant Nos. DMR 1720530 and CMMI-1548571).

REFERENCES

[1]Allison C Daley and Jonathan B Antcliffe. Evolution: The battle of the first animals. *Current Biology*, 29(7):R257–R259, 2019.

[2]Anthony K Redmond and Aoife McLysaght. Evidence for sponges as sister to all other animals from partitioned phylogenomics with mixture models and recoding. *Nature communications*, 12(1):1–14, 2021.

[3]Jasmine L Mah and Sally P Leys. Think like a sponge: the genetic signal of sensory cells in sponges. *Developmental biology*, 431(1):93–100, 2017.

[4]Casey W Dunn, Sally P Leys, and Steven HD Haddock. The hidden biology of sponges and ctenophores. *Trends in ecology & evolution*, 30(5):282–291, 2015.

[5]Robert Garrone. *Phylogenesis of connective tissue*. Karger Publishers, 1978.

[6]George Parker Bidder. Memoirs: The relation of the form of a sponge to its currents. *Journal of Cell Science*, 2(266):293–324, 1923.

[7]Sally P Leys, Gitai Yahel, Matthew A Reidenbach, Verena Tunnicliffe, Uri Shavit, and Henry M Reiswig. The sponge pump: the role of current induced flow in the design of the sponge body plan. *PloS one*, 6(12):e27787, 2011.

[8]Stephen R Palumbi. How body plans limit acclimation: Responses of a demosponge to wave force. *Ecology*, 67(1):208–214, 1986.

[9]Mark W Denny, Thomas L Daniel, and MAR Koehl. Mechanical limits to size in wave-swept organisms. *Ecological monographs*, 55(1):69–102, 1985.

[10]Michael A Monn and Haneesh Kesari. A new structure-property connection in the skeletal elements of the marine sponge tethya aurantia that guards against buckling instability. *Scientific reports*, 7(1):1–10, 2017.

[11]MAR Koehl. Mechanical design of spicule-reinforced connective tissue. *Journal of Experimental Biology*, 98(1):239–267, 1982.

[12]Dennis E Discher, Paul Janmey, and Yu-li Wang. Tissue cells feel and respond to the stiffness of their substrate. *Science*, 310(5751):1139–1143, 2005.

[13]Ovijit Chaudhuri, Justin Cooper-White, Paul A Janmey, David J Mooney, and Vivek B Shenoy. Effects of extracellular matrix viscoelasticity on cellular behaviour. *Nature*, 584 (7822):535–546, 2020.

[14]JR Xavier, PG Rachello-Dolmen, F Parra-Velandia, CHL Schönberg, JAJ Breeuwer, and RWM Van Soest. Molecular evidence of cryptic speciation in the "cosmopolitan" excavating sponge cliona celata (porifera, clionaidae). *Molecular phylogenetics and evolution*, 56 (1):13–20, 2010.

[15]John D Ferry. *Viscoelastic properties of polymers*. John Wiley & Sons, 1980.

[16]Alessandra Bonfanti, Jonathan Fouchard, Nargess Khalilgharibi, Guillaume Charras, and Alexandre Kabla. A unified rheological model for cells and cellularised materials. *Royal Society open science*, 7(1):190920, 2020.

[17]Jonathan Louis Kaplan, Alessandra Bonfanti, and Alexandre Kabla. Rheos. jl-a julia package for rheology data analysis. *arXiv preprint arXiv:2005.02538*, 2020.

[18]Randy H Ewoldt, Christian Clasen, Anette E Hosoi, and Gareth H McKinley. Rheological fingerprinting of gastropod pedal mucus and synthetic complex fluids for biomimicking adhesive locomotion. *Soft Matter*, 3(5):634–643, 2007.

[19]Kwang Soo Cho, Kyu Hyun, Kyung Hyun Ahn, and Seung Jong Lee. A geometrical interpretation of large amplitude oscillatory shear response. *Journal of rheology*, 49(3): 747–758, 2005.

[20]Nicholas A Kurniawan, Long Hui Wong, and Raj Rajagopalan. Early stiffening and softening of collagen: interplay of deformation mechanisms in biopolymer networks. *Biomacromolecules*, 13(3):691–698, 2012.

[21]Arezki Boudaoud, Agata Burian, Dorota Borowska-Wykret, Magalie Uyttewaal, Roman

Wrzalik, Dorota Kwiatkowska, and Olivier Hamant. Fibriltool, an imagej plug-in to quantify fibrillar structures in raw microscopy images. *Nature protocols*, 9(2):457–463, 2014.

[22]John NA Hooper and Rob WM van Soest. *Systema Porifera. A Guide to the Classification of Sponges*. Springer, 2002.

[23]Nicole Boury-Esnault and Klaus Rützler. Thesaurus of sponge morphology. *Smithsonian contributions to zoology*, 1997.

[24]Anne SG van Oosten, Xingyu Chen, LiKang Chin, Katrina Cruz, Alison E Patteson, Katarzyna Pogoda, Vivek B Shenoy, and Paul A Janmey. Emergence of tissue-like mechanics from fibrous networks confined by close-packed cells. *Nature*, 573(7772):96–101, 2019.

[25]Dawei Song, Jordan L Shivers, Fred C MacKintosh, Alison E Patteson, and Paul A Janmey. Cell-induced confinement effects in soft tissue mechanics. *Journal of Applied Physics*, 129 (14):140901, 2021.

[26]Katarzyna Pogoda, LiKang Chin, Penelope C Georges, FitzRoy J Byfield, Robert Bucki, Richard Kim, Michael Weaver, Rebecca G Wells, Cezary Marcinkiewicz, and Paul A Janmey. Compression stiffening of brain and its effect on mechanosensing by glioma cells. *New journal of physics*, 16(7):075002, 2014.

[27]L Angela Mihai, LiKang Chin, Paul A Janmey, and Alain Goriely. A comparison of hyperelastic constitutive models applicable to brain and fat tissues. *Journal of The Royal Society Interface*, 12(110):20150486, 2015.

[28]Maryna Perepelyuk, LiKang Chin, Xuan Cao, Anne van Oosten, Vivek B Shenoy, Paul A Janmey, and Rebecca G Wells. Normal and fibrotic rat livers demonstrate shear strain softening and compression stiffening. *PloS one*, 11(1):e0146588, 2016.

[29]TA Engstrom, K Pogoda, K Cruz, PA Janmey, and JM Schwarz. Compression stiffening in biological tissues: On the possibility of classic elasticity origins. *Physical Review E*, 99 (5):052413, 2019.

[30]Paula de Almeida, Paul A Janmey, and Paul HJ Kouwer. Fibrous hydrogels under multiaxial deformation: Persistence length as the main determinant of compression softening. *Advanced Functional Materials*, 31(18):2010527, 2021.

[31]Mahsa Vahabi, Abhinav Sharma, Albert James Licup, Anne SG Van Oosten, Peter A Galie, Paul A Janmey, and Fred C MacKintosh. Elasticity of fibrous networks under uniaxial prestress. *Soft matter*, 12(22):5050–5060, 2016.

[32]Alexander H.D. Cheng. *Poroelasticity*. Springer, 2016.

[33]George Neville Greaves, A Lindsay Greer, Roderic S Lakes, and Tanguy Rouxel. Poisson's ratio and modern materials. *Nature materials*, 10(11):823–837, 2011.

[34]Ray H Baughman. Auxetic materials: Avoiding the shrink. *Nature*, 425(6959):667–667, 2003.

[35]Paul A Janmey, Margaret E McCormick, Sebastian Rammensee, Jennifer L Leight, Penelope C Georges, and Fred C MacKintosh. Negative normal stress in semiflexible biopolymer gels. *Nature materials*, 6(1):48–51, 2007.

[36]Christine C Morrow, Niamh E Redmond, Bernard E Picton, Robert W Thacker, Allen G Collins, Christine A Maggs, Julia D Sigwart, and A Louise Allcock. Molecular phylogenies support homoplasy of multiple morphological characters used in the taxonomy of heteroscleromorpha. *Integrative and Comparative Biology*, 53(3):428–446, 2013.

[37]Eve Gazave, Sophie Carteron, Anne Chenuil, Evelyn Richelle-Maurer, Nicole Boury-Esnault, and Carole Borchiellini. Polyphyly of the genus axinella and of the family axinellidae. *Molecular Phylogenetics and Evolution*, 57(1):35–47, 2010.

[38]Arno P Schniewind and JD Barrett. Wood as a linear orthotropic viscoelastic material. *Wood Science and Technology*, 6(1):43–57, 1972.

[39]SC Cowin and MM Mehrabadi. Identification of the elastic symmetry of bone and other materials. *Journal of biomechanics*, 22(6-7):503–515, 1989.

[40]Simona Di Nino and Angelo Luongo. A simple homogenized orthotropic model for in-plane analysis of regular masonry walls. *International Journal of Solids and Structures*, 167:156–169, 2019.

[41]ML Gardel, Jennifer Hyunjong Shin, FC MacKintosh, L Mahadevan, Paul Matsudaira, and David A Weitz. Elastic behavior of cross-linked and bundled actin networks. *Science*, 304(5675):1301–1305, 2004.

[42]Belinda Alvarez, Rob WM van Soest, and Klaus Rützler. A revision of the axinellidae of the central-west atlantic region. *Smithsonian Contributions to Zoology*, 1998.

[43]Susanna López-Legentil, Patrick M Erwin, Timothy P Henkel, Tse-Lynn Loh, and Joseph R Pawlik. Phenotypic plasticity in the caribbean sponge callyspongia vaginalis. *Scientia Marina*, 74(3):445–453, 2010.

[44]RWM Van Soest. Demosponge higher taxa classification re-examined. In *Fossil and recent sponges*, pages 54–71. Springer, 1991.

[45]Carl P Goodrich, Simon Dagois-Bohy, Brian P Tighe, Martin Van Hecke, Andrea J Liu, and Sidney R Nagel. Jamming in finite systems: Stability, anisotropy, fluctuations, and scaling. *Physical Review E*, 90(2):022138, 2014.

[46]Steven Vogel. *Life in Moving Fluids: The Physical Biology of Flow*. Princeton University Press, 1994.

[47]L Oey, T Ezer, and H Lee. Loop current, rings and related circulation in the gulf of mexico: A review of numerical models and future challenges. *Geophysical Monograph-American Geophysical Union*, 161:31, 2005.

[48]Harry W Wells, Mary Jane Wells, and Irving Emery Gray. Marine sponges of north carolina. *Journal of the Elisha Mitchell Scientific Society*, 76(2):200–245, 1960.

[49]Henrik Ronellenfitsch. Optimal elasticity of biological networks. *Physical Review Letters*, 126(3):038101, 2021.

[50]Edward R Abraham. The fractal branching of an arborescent sponge. *Marine Biology*, 138(3):503–510, 2001.

[51]Jaap A Kaandorp and Janet E Kübler. *The algorithmic beauty of seaweeds, sponges and corals*. Springer Science & Business Media, 2001.

[52]Georgios Gounaris, Miguel Ruiz Garcia, and Eleni Katifori. Distribution efficiency and structure of complex networks. *arXiv preprint arXiv:2111.04657*, 2021.

[53]María-J Uriz, Xavier Turon, Mikel A Becerro, and Gemma Agell. Siliceous spicules and skeleton frameworks in sponges: origin, diversity, ultrastructural patterns, and biological functions. *Microscopy research and technique*, 62(4):279–299, 2003.

[54]Avigdor Abelson, Touvia Miloh, and Yossi Loya. Flow patterns induced by substrata and body morphologies of benthic organisms, and their roles in determining availability of food particles. *Limnology and Oceanography*, 38(6):1116–1124, 1993.

[55]Jordan L Shivers, Jingchen Feng, Anne SG van Oosten, Herbert Levine, Paul A Janmey, and Fred C MacKintosh. Compression stiffening of fibrous networks with stiff inclusions. *Proceedings of the National Academy of Sciences*, 117(35):21037–21044, 2020.

[56]Cornelis Storm, Jennifer J Pastore, Fred C MacKintosh, Tom C Lubensky, and Paul A Janmey. Nonlinear elasticity in biological gels. *Nature*, 435(7039):191–194, 2005.

[57]Chase P Broedersz and Fred C MacKintosh. Modeling semiflexible polymer networks. *Reviews of Modern Physics*, 86(3):995, 2014.

[58]Jerome Gross, Zelda Sokal, and Malcolm Rougvie. Structural and chemical studies on the

connective tissue of marine sponges. *Journal of Histochemistry & Cytochemistry*, 4(3): 227–246, 1956.

[59]Jean-Yves Exposito and Robert Garrone. Characterization of a fibrillar collagen gene in sponges reveals the early evolutionary appearance of two collagen gene families. *Proceedings of the National Academy of Sciences*, 87(17):6669–6673, 1990.

[60]Volker Gloeckner, Markus Wehrl, Lucas Moitinho-Silva, Christine Gernert, Peter Schupp, Joseph R Pawlik, Niels L Lindquist, Dirk Erpenbeck, Gert Wörheide, and Ute Hentschel. The hma-lma dichotomy revisited: an electron microscopical survey of 56 sponge species. *The Biological Bulletin*, 227(1):78–88, 2014.

[61]Alison E Patteson, Katarzyna Pogoda, Fitzroy J Byfield, Kalpana Mandal, Zofia Ostrowska-Podhorodecka, Elisabeth E Charrier, Peter A Galie, Piotr Deptuła, Robert Bucki, Christopher A McCulloch, et al. Loss of vimentin enhances cell motility through small confining spaces. *Small*, 15(50):1903180, 2019.

[62]Roderic Lakes. Foam structures with a negative poisson's ratio. *Science*, 235:1038–1041, 1987.

[63]Nathan C Keim, Joseph D Paulsen, Zorana Zeravcic, Srikanth Sastry, and Sidney R Nagel. Memory formation in matter. *Reviews of Modern Physics*, 91(3):035002, 2019.

[64]KL Galloway, EG Teich, XG Ma, Ch Kammer, IR Graham, NC Keim, C Reina, DJ Jerolmack, AG Yodh, and PE Arratia. Relationships between structure, memory and flow in sheared disordered materials. *Nature Physics*, 18(5):565–570, 2022.

[65]Eric M Schwen, Meera Ramaswamy, Chieh-Min Cheng, Linda Jan, and Itai Cohen. Embedding orthogonal memories in a colloidal gel through oscillatory shear. *Soft matter*, 16 (15):3746–3752, 2020.

[66]Konstantin Volokh. *Mechanics of soft materials*. Springer, 2016.

[67]Morteza Nejati, Marie Luise Texas Dambly, and Martin O Saar. A methodology to determine the elastic properties of anisotropic rocks from a single uniaxial compression test. *Journal of Rock Mechanics and Geotechnical Engineering*, 11(6):1166–1183, 2019.

[68]Ehsan Ban, Hailong Wang, J Matthew Franklin, Jan T Liphardt, Paul A Janmey, and Vivek B Shenoy. Strong triaxial coupling and anomalous poisson effect in collagen networks. *Proceedings of the National Academy of Sciences*, 116(14):6790–6799, 2019.

[69]Randy H Ewoldt. Defining nonlinear rheological material functions for oscillatory shear. *Journal of Rheology*, 57(1):177–195, 2013.

[70]Manfred Wilhelm, Pierre Reinheimer, and Martin Ortseifer. High sensitivity fourier-transform rheology. *Rheologica Acta*, 38(4):349–356, 1999.